NANO LETTERS

Letter

pubs.acs.org/NanoLett

Purely Coherent Nonlinear Optical Response in Solution Dispersions of Graphene Sheets

Rui Wu,[†] Yingli Zhang,[†] Shichao Yan,[†] Fei Bian,[†] Wenlong Wang,*[,†] Xuedong Bai,[†] Xinghua Lu,[†] Jimin Zhao,*[,†] and Enge Wang[‡]

[†]Beijing National Laboratory for Condensed Matter Physics and Institute of Physics, Chinese Academy of Sciences, Beijing 100190, China

[‡]International Center for Quantum Materials, School of Physics, Peking University, Beijing 100871, China

Supporting Information

ABSTRACT: We have developed an efficient chemical exfoliation approach for the high-throughput synthesis of solution-processable, high-quality graphene sheets that are noncovalently functionalized by alkylamine. Purely coherent nonlinear optical response of these graphene sheets has been investigated, using near-infrared, visible, and ultraviolet continous wave and ultrafast laser beams. Spatial self-phase modulation has been unambiguously observed in the solution dispersions. Our results suggest that this coherent light scattering is due to a broadband, ultrafast, and remarkably huge third-order optical nonlinearity $\chi^{(3)}$, which is a manifestation of the graphene's cone-shaped large-energy-scale band structure. Our experimental findings endow graphene new potentials in nonlinear optical applications.

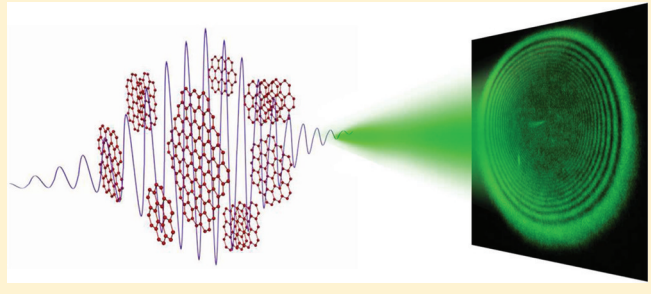

KEYWORDS: *Graphene, noncovalent functionalization, chemical exfoliation, ultrafast, self-phase modulation, coherent*

The experimental discovery of graphene in 2004 has evoked ever-increasing scientific interest in this remarkable two-dimensional (2D) material.[1] Apart from its peculiar electronic structures leading to interesting fundamental physics, graphene has also outstanding material properties ranging from ultrahigh carrier mobility to extreme mechanical stiffness, which promises a plethora of potential applications including nanoelectronic circuits, sensors, conductive films, reinforced composite materials, and many others. As a versatile experimental means, optical spectroscopy has been widely used to investigate the optical conductivity, electronic structure, and charge dynamics of single-, double-, and few-layer graphene sheets.[2−9] Although the pioneering experiments extensively used infrared and terahertz radiation, the large-energy-scale conical-shaped band structure indicates that the linear and nonlinear optical properties of graphene may also be investigated in the near-infrared, visible, and even ultraviolet regions. Ultrafast lasers have also been used to explore the carrier dynamics and multiparticle interaction.[6,10−13] However, so far most optical investigations of graphene have focused on reflection, transmission, absorption, spontaneous Raman- and Rayleigh-type light scatterings.[2−14] Very little has been reported on purely coherent light scattering of graphene, except for one four-wave mixing experiment in the near-infrared region.[15] Here we report a novel approach in revealing purely coherent optical behavior arising from the nonlinearity of graphene in a region ranging from ultraviolet to near-infrared. For the first time, we observed the spatial self-phase modulation (SSPM) of graphene, which is broad band, ultrafast as suggested by our results, and remarkably huge.

The full exploitation and application of the unique properties of graphene materials will rely largely on their high-throughput synthesis and successful processing. Of particular importance is the development of proper chemical functionalization strategies, either covalent or noncovalent, for graphene sheets to render them amenable to solution-processing and solution-phase analyses. Here we report an efficient chemical exfoliation approach for the high-throughput synthesis of high-quality graphene sheets that are noncovalently functionalized with alkylamine. As a consequence of the surface attachment of alkyl tails, the functionalized sheets show enhanced solution processablity and can form stable colloidal dispersion in a variety of common organic solvents, including butanol, tetrahydrofuran (THF), *N*,*N*-dimethylformamide (DMF), *N*-methyl-2-pyrrolidinone (NMP), and chloroform ($CHCl_3$). Moreover, from the solution dispersions, we unambiguously observed SSPM. Broadband and ultrafast optical coherence led to nonlinear light scattering into multiple unique conical diffraction rings, which manifests the strongly anisotropic microscopic structure of the dispersion sample composed of this two-dimensional carbon material. Furthermore, an excep-

Received: July 10, 2011
Revised: October 19, 2011
Published: November 17, 2011

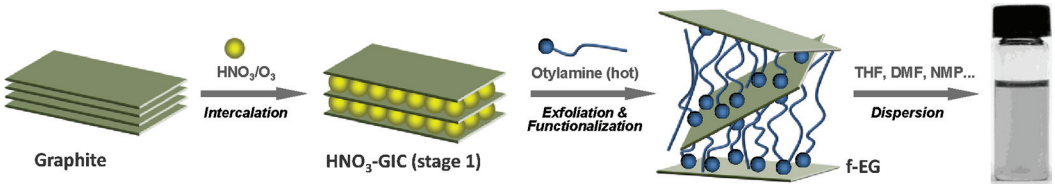

Figure 1. Schematic diagram showing the intercalation, exfoliation, and functionalization processes to produce the graphene sheets that are dispersible in a variety of organic solvents.

tionally large third-order nonlinearity $\chi^{(3)}$ and a very low laser intensity threshold I_{th} have been obtained with both continuous wave (cw) and ultrafast pulsed laser beams. Through comparison with other materials, especially low-dimensional carbon materials, the physical origin of these properties is explained in connection with the Dirac-cone band structure of graphene sheets. These fundamental physical properties endow graphene-related materials with great potential in various nonlinear optical applications, especially in the visible and ultraviolet region, such as optical switches and optical limiting devices that were previously made with other materials.

Spatial self-phase modulation was originally observed in nematic liquid-crystal films in the early 1980s,[16] then later in C_{60}-benzene solutions[17] and many other materials.[18−20] Like other nonlinear optical processes such as four-wave mixing, SSPM is a manifestation of the coherent response of the material. We would therefore expect that it could also be observed in ultrafast optical measurements, but so far there have been few reports on this. We shall show that this may be observed using femtosecond laser pulses of different central wavelengths.

The general strategy for producing alkylamine-functionalized graphene is shown in Figure 1. The initial step involves the intercalation of graphite flakes with nitric acid (HNO_3) to form the first stage graphite intercalation compound (GIC),[21] according to a previously reported procedure with the use of ozone (O_3) as oxidant.[22] Experimentally, approximately 100 mg of natural flake graphite (80 mesh, Nan-Shu Graphite Co. Ltd., Qingdao, China) was soaked in ∼10 mL of fuming nitric acid at 50 °C under mild stirring in a glass flask, where ozone-enriched oxygen from a laboratory ozonizer (ozone content in the gas flow ∼8 vol %) was bubbled through the reaction mixture. Over time, the color of the graphite in the reactor gradually changed from black to clear blue, indicating formation of stage-1 HNO_3-GIC (alternating layers of graphene and intercalant). The ozone flow was continued until all the graphite turned blue. After intercalation, the reaction mixture was immediately vacuum-filtered with a 1 μm pore size PTFE membrane filter to remove the superfluous nitric acid. The resultant stage-1 HNO_3-GIC solid with a characteristic clear-blue color was then rapidly transferred into a glass flask containing ∼50 mL of octylamine (OA) that was preheated at 150 °C. Upon contact with hot OA, the HNO_3-GIC underwent vigorous decomposition producing large amounts of heat and gas, which caused a high degree of exfoliation of the graphene sheets. With further treatment of the sheets in hot OA for an extended duration (∼10 h) under continuous stirring, the noncovalent surface functionalization of the exfoliated graphene sheets by OA was thus "one-pot" accomplished, thereby producing the OA-functionalized, exfoliated graphene (f-EG). The solid f-EG was then collected by filtration and extensively washed with water−ethanol mixture and then pure ethanol.

A key step of the whole synthesis process is the liquid-phase expansion of stage-1 HNO_3-GIC in hot OA to form f-EG. Compared with the starting graphite flakes as well as the densely packed HNO_3-GICs, the f-EG solid occupies a considerably larger volume with a characteristic fluffy appearance. A typical scanning electron micrograph (SEM) of f-EG is displayed in the inset of Supporting Information Figure S1a. Thermogravimetric analysis has been performed under air flow to compare the thermal stability of f-EG relative to that of the initial pure graphite and also to assess the amount of OA that is noncovalently bonded onto the exfoliated graphene sheets. As shown in Supporting Information Figure S1a, the starting pure graphite has an oxidation onset at around 750 °C and is completely oxidized to carbon dioxide close to 1000 °C. The thermogram of f-EG, on the other hand, is very different. The first region of mass loss of f-EG occurs at temperatures below 150 °C and is attributed to the removal of absorbed water and ethanol during washing. Note that the presence of the large amount (∼25 wt %) of absorbed solvents is indicative of the large surface area of f-EG, which is consistent with the SEM imaging results. The next approximately 20 wt % of mass loss occurring within the temperature range of 150−400 °C is associated with the release and subsequent oxidative decomposition of the organic OA molecules that are noncovalently attached onto the exfoliated graphene sheets. Finally, the bulk material of graphitic carbon is progressively oxidized within 425−800 °C, a temperature range distinctly lower than that of the original pure graphite flakes. This result verifies again the fact that f-EG consists of highly exfoliated graphene sheets that are much more prone to oxidation than the tightly stacked graphite flakes.

With the aid of bath-sonication for about 1 h, the f-EG solid can be easily dispersed in a variety of common organic solvents such as butanol, THF, DMF, NMP, and chloroform. After mild centrifugation (1000 rpm, 1 h) of the resultant suspension to remove the larger and/or thicker flakes or any larger aggregates, the homogeneous and stable colloidal dispersions of OA-functionalized graphene sheets in these solvents can be obtained, as shown in Supporting Information Figure S1b. Typically, the solubility of OA-functionalized graphene in these five tested solvents is in the order of NMP > DMF > THF > butanol> chloroform.

Transmission electron microscopy (TEM) in a JEOL 2010F at an accelerating voltage of 200 kV was then employed to characterize the exact form of graphene sheets in the solution dispersions. Since the highest degree of dispersion is achieved in NMP, the specimens for TEM imaging were prepared by dropping the NMP dispersion onto holey carbon mesh grids. Shown in Figure 2a−c are typical TEM images of the OA-functionalized graphene sheets. The number of graphene layers was confirmed by high-resolution TEM imaging of the folded edges,[23] as depicted in the inset of each image. A histogram of the distribution of the number of layers is shown in Figure 2d.

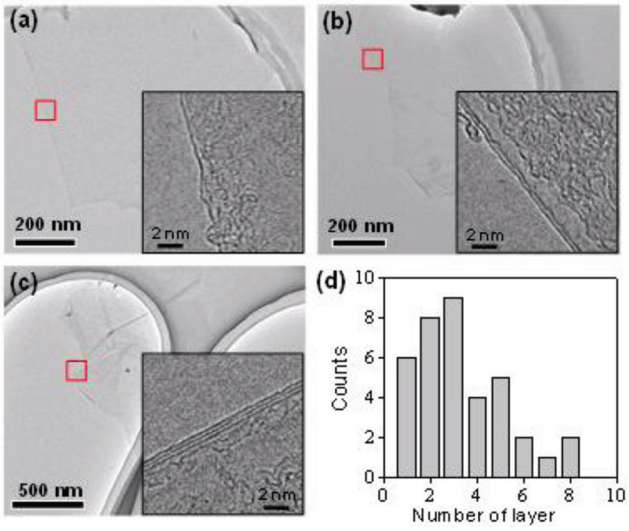

Figure 2. Typical TEM images of (a) single-, (b) double- and (c) trilayer graphene sheets deposited from the NMP dispersion. Insets in each picture are the corresponding HRTEM images (zoom-in of squares) showing the folded edges of the targeted graphene sheets. (d) Histogram of the graphene layers in the sample.

Typically, the graphene sheets were ~1−3 μm in size, and nearly all were found to be less than 10 layer thick, with more than 60% being 1−3 layers. Raman spectra were also taken to verify the high-quality of the OA-functionalized graphene sheets. The measurements were carried out on thin films of graphene sheets deposited by vacuum filtration of the dispersions through porous alumina membranes.[24] Comparison of the Raman spectra at 532 nm for graphene and the starting bulk graphite is displayed in Supporting Information Figure S2. As expected, the characteristic shape of the 2D band of graphene suggests that the average number of layers is less than five.[25] We see that the lack of broadening of the G band confirms that the graphene sheets are virtually defect-free. Note that the appearance of the small D band is due to sheet edges rather than structural defects or disorders in the basal plane, since the laser spot size was 1−2 μm so there were always a large quantity of edges illuminated by the beam.

In the nonlinear optical experiment, a quartz cuvette of 1 cm thickness was used to contain the graphene dispersion solution in NMP. A linearly polarized beam from a 532 nm TEM_{00}-mode cw laser was focused onto the graphene suspension by a lens of focal length 100 mm. The distance between the lens and the front surface of the cuvette was 65 mm. The $1/e^2$ intensity diameter of the laser beam at the lens was 1.8 mm and 630 μm at the front surface of the cuvette. Inside the sample, due to self-focusing, the beam converged rapidly to reach a minimum diameter after a propagation length of a few millimeters. Then it continued like a plane wave, though with a progressively slightly increasing diameter as its intensity decreased due to weak absorption and light scattering. After exiting the cuvette, the beam began to diverge into conical diffraction rings, which were projected on a white screen placed 430 cm away behind the sample. Figure 3a is a photograph showing a typical pattern of the diffraction rings, taken with a CCD camera (Nikon P5100). It can be seen that the outermost ring has the strongest intensity and thickest width, the fringe intensity and width both decreasing toward the center. The intensity distribution is

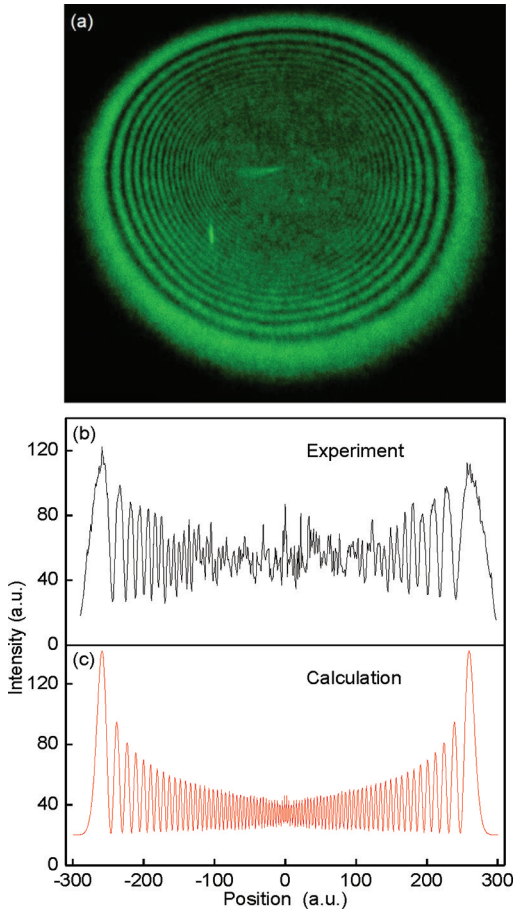

Figure 3. (a) Photograph of a typical SSPM diffraction ring pattern, where the incident light was a 532 nm TEM_{00} cw laser beam. (b) Radial intensity distribution of the diffraction rings shown in Figure 2a. (c) Theoretical calculation result; a. u. represents arbitrary units.

plotted in Figure 3b, which compares well with our numerical calculation results in Figure 3c.

Next we investigated the intensity dependence of the nonlinear effect. With increased laser power, more rings were observed, as if they were emerging from the center of the pattern and all their diameters became enlarged gradually. The number of rings increases nearly linearly with the incident intensity, as shown in Figure 4, and no sign of sharp saturation was seen below 100 W/cm^2. The diameter of the outermost ring also increased almost linearly, as illustrated in the inset of Figure 4. It can be seen that the intensity threshold for observing the diffraction rings is about 12.5 W/cm^2. It is interesting that when the laser beam was directly incident on the sample without focusing, diffraction rings were also observed, and in particular with a sharply reduced threshold of only 0.6 W/cm^2 (marked in red in Figure 4). This remarkable decrease of the threshold in observing the rings is mainly due to the enclosure of more graphene sheets inside the active illuminated area of the unfocused beam. As will be explained below, this is a coherent nonlinear optical process, where photons generated from different sheets constructively interfere and enhance the intensity of the ring patterns on the screen.

Parallel experiments in graphene solution in DMF were also carried out. We observed similar SSPM phenomena to those in NMP. Because the maximum graphene sheet concentration in

dx.doi.org/10.1021/nl2023405 | Nano Lett. 2011, 11, 5159−5164

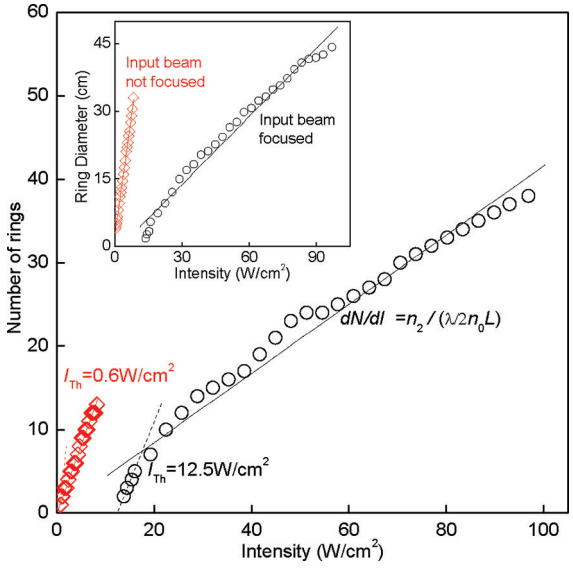

Figure 4. Dependence of the number of rings on the laser intensity. The intensity threshold for observing diffraction rings is about 12.5 W/cm^2 for the focused beam (black circles) and 0.6 W/cm^2 for the unfocused beam (red squares). Inset: dependence of the outermost ring diameter on the laser intensity. The straight lines are linear fits.

DMF is much smaller than in NMP, the corresponding number and outermost diameter of the rings are also smaller. Furthermore, in a control experiment with NMP solvent only, no diffraction pattern was observed. On the basis of these experiments, we ascribe the diffraction rings to be due to the nonlinear optical properties of the graphene sheets, that is, the spatial self-phase modulation. When a laser beam traverses a nonlinear optical medium, the refractive index is a function of the intensity distribution. In terms of the third order nonlinearity, the refractive index can be expressed as $n = n_0+n_2I$, where n_0 and n_2 are the linear and nonlinear refractive indexes. The phase shift $\Delta\psi$ of the laser beam after passing through a graphene suspension of thickness L is

$$\Delta\psi(r) = \left(\frac{2\pi n_0}{\lambda}\right)\int_0^L n_2 I(r, z)\mathrm{d}z \tag{1}$$

where r is the radial coordinate, λ is the laser wavelength in vacuum, L is the total propagation length contributing to the spatial self-phase modulation, and $I(r, z)$ the intensity distribution. For a Gaussian beam, the intensity $I(0, z)$ at the center is twice of the average intensity I measured in the experiment, and $\Delta\psi(r) \approx \Delta\psi_0 \exp(-2r^2/a^2)$, where a is the $1/e^2$ beam radius. The total number of rings N is determined by $[\Delta\psi(0) - \Delta\psi(\infty)] = 2N\pi$ for a given laser intensity.[16] Thus, after a simple derivation, we have

$$n_2 = \left(\frac{\lambda}{2n_0L}\right)\frac{N}{I} \tag{2}$$

In our experiment N is approximately proportional to I, thus the nonlinearity n_2 can be easily obtained by finding N/I at the maximum laser power in Figure 4. Taking L = 3 mm and n_0 = 1.47, we obtain $n_2 = 2.5 \times 10^{-9}$ m^2/W for the focused laser beam experiment. The value of n_2 for the unfocused experiment is of the same order, being 3×10^{-9} m^2/W. Since $n_2 = (12\pi^2/n_0^2c)10^3\chi^{(3)}$, we can estimate the magnitude of the effective third-order nonlinear susceptibility $\chi^{(3)}$ to be in the order of 1×10^{-3} (e.s.u.) for the graphene dispersion solution. It is instructive to compare this optical nonlinearity for our bulk solution with that of single-layer graphene measured in a previous four-wave mixing experiment.[15] We now give a qualitative estimate based on the coherent behavior of the SSPM process. From $n = n_0 + n_2I$, we know that the refractive index, thus approximately the diffraction angle, is proportional to the intensity, which is also reflected in eq 1. Since $E_{\text{total}} = \sum_{i=1}^{M} E_i \approx ME_{\text{single layer}}$, where M is the effective number of the graphene layers, we have $I_{\text{total}} \approx M^2 I_{\text{single layer}}$. Therefore, qualitatively, we estimate that $\chi^{(3)}_{\text{total}} \approx M^2\, \chi^{(3)}_{\text{single layer}}$. In our experiment M is on the order of 100 (see Supporting Information S4), thus the estimated $\chi^{(3)}_{\text{single layer}}$ is of the order of 1×10^{-7} (e.s.u.), which compares well with the result in ref 15. Considering the complexity of a solution, our heuristic interpretation might be subject to further verification. Since we have $D \propto n_0 n_2 I s/\lambda$ with s being the distance between the sample and the screen, the proportionality relation between D and I is also obtained, which is illustrated in the inset of Figure 4.

To get an idea about the magnitude of this optical nonlinearity, we show in the Supporting Information S3 that it is larger than all previously reported carbon-based materials, such as carbon nanotube and C_{60}. Moreover, the threshold for observing the diffraction rings is lower than that of any of the other materials reported to exhibit SSPM. Nonetheless, based on the similarity in band structure, we expect that suspensions of thin graphite flakes or microcrystalline graphitic materials also preserve similar enhanced nonlinearities.

We also employed ultrafast laser pulses to investigate the SSPM at different wavelengths. The laser pulses had a central wavelength of 800 nm, repetition rate of 250 kHz and a pulse duration of 80 fs (Micra seeded RegA-9050 Ti:sapphire laser amplifier, Coherent Inc.). First, 400 nm laser pulses was generated through a nonlinear crystal, which was then used for sum frequency generation with the 800 nm pulses to produce 267 nm pulses. This home-built 267 nm laser source had a power of a few milliwatts and was focused onto the sample with a 10 cm focusing lens. The observed SSPM diffraction rings were very clear on the white screen. The digital camera we used to take the photos was not very sensitive to the 267 nm light, but after contrast ratio adjustment (Figure 5b−d) the image quality approached that observed by the naked eye (viewed at a distance). Figure 5a−d shows the original and enhanced images in which we can see typical features of SSPM. The interesting aspect about the 267 nm photon is that it has an energy (4.65 eV) in resonance with the π-plasmon mode (4.7 eV) of free-standing single-layer graphene films.[26] Thus the threshold is relatively low compared with those for other wavelengths. It is worthy to note that although SSPM diffraction has been observed at 514.5, 532, and 632.8 nm in different materials, there has been no report at such a high photon energy. To further probe this broadband SSPM property, we used the original 800 nm ultrashort laser pulses with an average power of about 30 mW to perform a similar experiment. As expected, SSPM was also observed, and is shown in Figure 5f. However, the rings were somewhat deformed, as was also observed in the 532 nm cw laser experiment (Figure 5e). What is interesting is that originally perfect ring-shaped fringes appeared but after about one second they deformed into the stable patterns shown in Figure 5e,f. The same also applies to Figure 3a. We ascribe this phenomenon to thermal effects (see Supporting Information S5).

dx.doi.org/10.1021/nl2023405 | Nano Lett. 2011, 11, 5159−5164

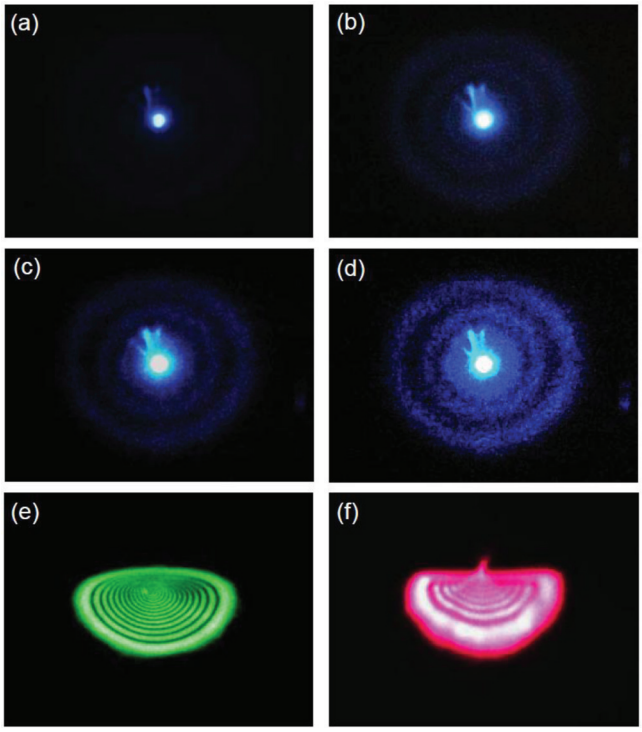

Figure 5. The SSPM patterns observed at different wavelengths. (a) Original photo taken with 267 nm ultrafast laser pulses. (b–d) Images based on (a) after enhancement. (e) Photo taken with 532 nm cw laser beam. (f) Photo taken with 800 nm ultrafast laser pulses.

To understand how light at different wavelengths could generate this effect, we plot the light–graphene interaction in Figure 6a. The origin of the optical nonlinearity may be

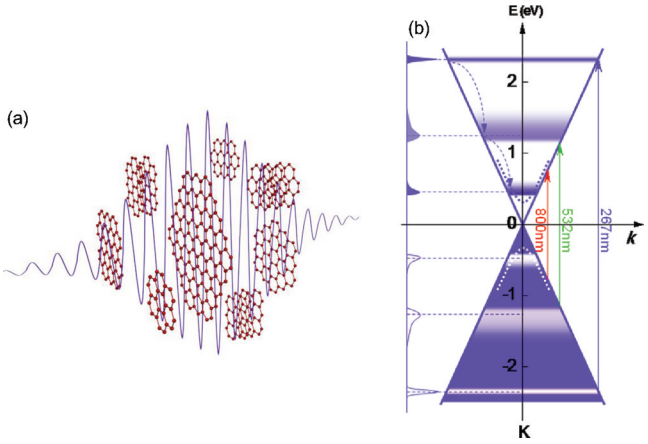

Figure 6. Micromechanism for the observation of SSPM. (a) Schematic showing the alignment of electron motion and graphene sheets in an incident field, where light propagates from left to right. Electrons oscillate with the field. (b) Band structure that allows broad spectrum excitation of free carriers, which contributes instantly and later to the n_2 nonlinearity. The dashed lines represent the band structure of bilayer and other few-layer graphene sheets.

attributed to the reorientation and alignment of the graphene sheets induced by the electromagnetic field, which is similar to the case of liquid crystals.[16] Here the reorientation comes from the electron motion associated with the oscillating electric field of the incident light. As illustrated in Figure 6b, an electron in the valence band absorbs one incident photon and is excited to the conduction band through an interband transition. It subsequently relaxes back to the bottom of the cone on two different time scales. In the initial few hundreds of femtoseconds, carrier–carrier scattering is the major relaxation mechanism, then during the following few picoseconds, carrier–phonon relaxation becomes dominant, whereby the electrons settle down near the bottom of the band structure.[5,20–22] Whenever the laser light is present, the generated electrons and holes move in opposite directions, being antiparallel and parallel to the electric field, respectively. This results in a polarized graphene sheet.[27] Initially there might be an angle between this polarization and the electric field, associated with the interaction energy. Reorientation of the graphene sheets aligns them while minimizing the interaction energy. Alignment also comes from the plasmonic interaction between the graphene sheets, which is due to the giant intrinsic charge mobility caused by the dislocalization of the π-electrons.[1,28,29] The essential point is that the carriers within different sheets are perfectly in phase, that is, coherent, in the light field, thus each sheet contributes constructively to the SSPM ring patterns.

In concluding that the SSPM obtained using ultrafast laser pulses is a transient phenomena rather than a slow average effect, we note that it requires a well-defined fixed phase difference between photons so that interference can occur and diffraction can emerge in a direction outside the incident beam. Since the charge carriers relax within a few picoseconds and the temporal slot between each pulse is 4 μs, there cannot be interference between different pulses. Nearly all the coherence comes from each single pulse's self-phase-modulation. For the cw laser beam the coherence between photons is also restricted by the carrier relaxation time. We contemplate on the magnitude of the optical nonlinearity induced by ultrafast and cw laser beams. There is no huge difference between the ultrafast and cw SSPM measurements if the total average power is the same because due to time-integration effect, spatial enhancement of coherence, and low threshold, nearly every free carrier contributes equivalently to SSPM. It is roughly the total number of the generated free carriers that affects the observable nonlinearity. Note that we do not have two-photon or multiphoton processes here in generating the free carriers. In our experiment we did observe at the same average power nearly equal number of rings for cw and pulse beams, respectively.

To investigate the broadband feature, we show the energy band structure of the graphene sheets in Figure 6b. We see that the 800, 532, and 267 nm photons all fall into the conical regime of the band structure so they all can excite electrons that then delocalize and move under interaction with the light field. In our experiment, there are also bilayer and few-layer graphene sheets. Their band structures are different from that of a single-layer graphene crystal, marked by gaps at the K (K') points in momentum space.[30] The composition of chiral massless and massive fermions also varies for an even and odd number of layers.[30–32] The gap can be as large as a few hundred millielectronvolts.[2,3] For energies higher than this, the phonon bottleneck effect will be nearly the same for all the wavelengths we used, since the excited carriers relax close to the bottom in only a few picoseconds. From this analysis we believe that the broadband feature of our sample persists even for longer wavelengths, at least up to 1.5 μm.[2]

dx.doi.org/10.1021/nl2023405 | Nano Lett. 2011, 11, 5159–5164

To conclude, we have reported the high-throughput synthesis of alkylamine functionalized few-layer graphene sheets and a novel approach for investigating the coherence properties of their optical nonlinearity. We have observed broadband and ultrafast (as suggested by our results) SSPM from their solution dispersions, which is clearly due to coherent interference. We show that graphene layers in solution dispersions demonstrate exceptionally huge third-order optical nonlinearity. Our experiment extends the investigation of the coherent nonlinear optical properties of graphene to the visible and ultraviolet regions. Graphene may prove to be an ideal candidate for nonlinear optical applications, especially where SSPM plays an essential role.

■ ASSOCIATED CONTENT

Ⓢ Supporting Information

Additional figures on sample characterization, including optical transmission, and additional tables on the nonlinear refractive index n_2 and intensity threshold I_{th} as a comparison with those of other reported materials. This material is available free of charge via the Internet at http://pubs.acs.org.

■ AUTHOR INFORMATION

Corresponding Author

*E-mail: (W.W.) wwl@iphy.ac.cn; (J.Z.) jmzhao@iphy.ac.cn.

■ ACKNOWLEDGMENTS

We acknowledge useful discussions with Ling-An Wu, Nai-Hang Kwong, Jiming Bao, and P. M. Fu. This work was financially supported by the Natural Science Foundation of China (10704085, 10974246, 20973195) and the National Basic Research Program of China (2007CB936804, 2012CB821402).

■ REFERENCES

(1) Geim, A. K.; Novoselov, K. S. *Nat. Mater.* **2007**, *6*, 183.
(2) Mak, K. F.; Matthew, Y. S.; James, A. M.; Heinz, T. F. *Proc. Natl. Acad. Sci. U.S.A.* **2010**, *107*, 14999.
(3) Wang, F.; Zhang, Y. B.; Tian, C. S.; Girit, C.; Zettl, A.; Crommie, M.; Shen, Y. R. *Science* **2008**, *320*, 206.
(4) Li, Z. Q.; Henriksen, E. A.; Jiang, Z.; Hao, Z.; Martin, M. C.; Kim, P.; Stormer, H. L.; Basov, D. N. *Nat. Phys.* **2008**, *4*, 532.
(5) Mak, K. F.; Sfeir, M. Y.; Wu, Y.; Liu, C. H.; Misewich, J. A.; Heinz, T. F. *Phys. Rev. Lett.* **2008**, *101*, 196405.
(6) George, P. A.; Strait, J.; Dawlaty, J.; Shivarama, S.; Chandrashekhar, M.; Rana, F.; Spencer, M. G. *Nano Lett.* **2008**, *8*, 4248.
(7) Geng, B. S.; Horng, J.; Zhang, Y. B.; Tang, T. T.; Park, C. H.; Girit, C.; Hao, Z.; Martin, M.; Zettl, A.; Crommie, M.; Louie, S.; Wang, F. *Phys. Status Solidi B* **2010**, *247*, 2931.
(8) Shi, S. F.; Xu, X. D.; Ralph, D. C.; McEuen, P. L. *Nano Lett.* **2011**, *11*, 1814.
(9) Liu, Z. H.; Lu, X. X.; Peng, P.; Wu, W.; Pei, S. S.; Yu, Q. K.; Bao, J. M. *Phys. Rev. B* **2010**, *82*, 155435.
(10) Sun, D.; Wu, Z. K.; Divin, C.; Li, X. B.; Berger, C.; de Heer, W. A.; First, P. N.; Norris, T. B. *Phys. Rev. Lett.* **2008**, *101*, 157402.
(11) Newson, R. W.; Dean, J.; Schmidt, B.; van Driel, H. M. *Opt. Expr.* **2009**, *17*, 2326.
(12) Dawlaty, J. M.; Shivaraman, S.; Chandrashekhar, M.; Rana, F.; Spencer, M. G. *Appl. Phys. Lett.* **2008**, *92*, 042116.
(13) Kumar, S.; Anija, M.; Kamaraju, N.; Vasu, K. S.; Subrahmanyam, K. S.; Sood, A. K.; Rao, C. N. R. *Appl. Phys. Lett.* **2009**, *95*, 191911.
(14) Wang, J.; Hernandez, Y.; Lotya, M.; Coleman, J. N.; Blau, W. J. *Adv. Mater.* **2009**, *21*, 2430.
(15) Hendry, E.; Hale, P. J.; Moger, J.; Savchenko, A. K. *Phys. Rev. Lett.* **2010**, *105*, 097401.
(16) Durbin, S. D.; Arakelian, S. M.; Shen, Y. R. *Opt. Lett.* **1981**, *6*, 411.
(17) Han, Y. N.; Zhang, W. J.; Dong, F. Z.; Xia, Y. X.; Zang, W. C.; Yang, P.; Gu, G.; Du, Y. W.; Feng, D. *Chin. Phys. Lett.* **1992**, *9*, 647.
(18) Horowitz, M.; Daisy, R.; Werner, O.; Fisher, B. *Opt. Lett.* **1992**, *17*, 475.
(19) Yang, X. Q.; Qi, S. W.; Zhang, C. Z.; Chen, K.; Liang, X.; Yang, G.; Xu, T.; Han, Y.; Tian, J. G. *Opt. Commun.* **2005**, *256*, 414.
(20) Henari, F. Z.; Al-Saie, A. *Laser Phys.* **2006**, *16*, 1664.
(21) Dresselhaus, M. S.; Dresselhaus, G. *Adv. Phys.* **1981**, *30*, 139.
(22) Savoskin, M. V.; Mochalin, V. N.; Yaroshenko, A. P.; Lazareva, N. I.; Konstantinova, T. E.; Barsukov, I. V.; Prokofiev, I. G. *Carbon* **2007**, *45*, 2797.
(23) Gass, M. H.; Bangert, U.; Bleloch, A. L.; Wang, P.; Nair, R. R.; Geim, A. K. *Nat. Nanotechnol.* **2008**, *3*, 676.
(24) Hernandez, Y.; Nicolosi, V.; Lotya, M.; Blighe, F. M.; Sun, Z.; De, S.; McGovern, I. T.; Holland, B.; Byrne, M.; Gun'ko, Y. K.; Boland, J. J.; Niraj, P.; Duesberg, G.; Krishnamurthy, S.; Goodhue, R.; Hutchison, J.; Scardaci, V.; Ferrari, A. C.; Coleman, J. N. *Nat. Nanotechnol.* **2008**, *3*, 563.
(25) Ferrari, A. C.; Meyer, J. C.; Scardaci, V.; Casiraghi, C.; Lazzeri, M.; Mauri, F.; Piscanec, S.; Jiang, D. *Phys. Rev. Lett.* **2006**, *97*, 187401.
(26) Eberlein, T.; Bangert, U.; Nair, R. R.; Jones, R.; Gass, M.; Bleloch, A. L.; Novoselov, K. S.; Geim, A.; Briddon, P. R. *Phys. Rev. B* **2008**, *77*, 233406.
(27) Wang, Z. *Carbon* **2009**, *47*, 3050.
(28) Katsnelson, M. I. *Mater. Today* **2007**, *10*, 20.
(29) Geim, A. K. *Science* **2009**, *324*, 1530.
(30) Partones, B.; Peeters, F. M. *Phys. Rev. B* **2006**, *74*, 075404.
(31) Koshino, M.; Ando, T. *Phys. Rev. B* **2007**, *76*, 085425.
(32) Min, H. K.; MacDonald, A. H. *Phys. Rev. B* **2008**, *77*, 155416.